15th IFK
Proc. of the 15th International Fluid Power Conference <Symposium/Conference>
<DOI>

Motion Control of Multi-DOF Hydraulic Manipulator Driven by Independent Metering System with Friction Compensation

Yangxiu Xia[1], Litong Lyu[2,*], Bobo Helian[3], Zheng Chen[1]

[1] *Ocean College, Zhejiang University, 1 Zheda Road, Zhoushan, Zhejiang 316021, P. R. China*
[2] *School of Mechanical Engineering, Shijiazhuang Tiedao University, 17 North Second Ring East Road, Shijiazhuang, Hebei 050043, P. R. China*
[3] *Institute of Mobile Machines, Karlsruhe Institute of Technology, Kaiserstr. 12, 76131 Karlsruhe, Germany*

* Corresponding author: Tel.: +86-15267008148; E-mail address: litong_lyu@stdu.edu.cn

Abstract.

Multi-degree-of-freedom hydraulic manipulators are widely used in heavy-duty machinery, due to the advantages of hydraulic transmission. While previous research focused on output force and power, recent developments have shifted toward control performance and energy efficiency. However, precise control remains challenging for hydraulic manipulators compared to electric manipulators, due to the complexities of hydraulic transmission and multi-body dynamics. Nonlinear model-based control strategies and independent metering techniques have shown promise in overcoming these challenges. This paper investigates the motion control of a multi-DOF hydraulic manipulator driven by an independent metering system. A hydraulic circuit based on independent metering is designed, and the system's dynamics are modeled. To address nonlinearities, uncertainties, and friction in the system, an adaptive robust control strategy is proposed. Friction, which plays a significant role in degrading control performance, is compensated using the LuGre model-based approach. The proposed method is evaluated through simulations and experiments on a 4-DOF hydraulic manipulator test rig. Quantitative analysis, including the Integral of Time-weighted Absolute Error (ITAE) and maximum tracking errors, verifies that the proposed strategy achieves improved tracking performance and energy efficiency compared to traditional control methods.

Keywords. Independent metering system, hydraulic manipulator, motion control, friction compensation

1. INTRODUCTION

Multiple degrees of freedom (multi-DOF) hydraulic manipulators are typically installed on heavy-duty machinery like excavators [1] and Autonomous Underwater Vehicles (AUVs) [2] due to the benefits offered by hydraulic transmission systems. Historically, the primary focus regarding hydraulic manipulators has been on high output force/power [3], with limited attention given to studying control performance. This is because most machines were traditionally operated by operators controlling the valve orifices directly, without the application of closed-loop control systems. Nowadays, the control performance has emerged as a primary concern for hydraulic manipulators, given that fully-autonomous or semi-autonomous off-road machinery represents a significant research focus in numerous countries within the framework of intelligent development [4].

Unlike electric manipulators utilized in industrial applications, which employ servo motors to control the joints and therefore achieve higher control performance relatively easily, multi-DOF hydraulic manipulators typically utilize cylinders to drive the rotary joints instead of hydraulic motors [4]. As a result, precise control of hydraulic manipulators is more challenging due to the complex nature of hydraulic transmission and the multi-body mechanism. The dynamics of multi-DOF hydraulic manipulator is highly nonlinear with various uncertainties [5]. To attain high precision, nonlinear model-based control methods such as adaptive control or robust control have been proven effective [6, 7]. These control strategies aim to compensate for the nonlinear dynamics as accurately as possible and incorporate robust feedback mechanisms to address uncertainties and disturbances. Notably, friction represents a key nonlinear property within the dynamics of hydraulic manipulators [8]. Friction exhibits a complex relationship with velocity, particularly at low speeds [9]. Due to the kinematics of the hydraulic manipulator, when the end-effector is moving continuously and relatively fast, some joints may experience frequent stop-and-go or low speed motions. Inadequate compensation for such behaviors can lead to significant peak errors in the joints and degrade overall control performance.

Typically, the friction force is represented as a combination of Coulomb and viscous terms [10]. This model is accurate when the velocity is relatively high and can be easily integrated into model compensation control. However, as the velocity decreases, the discrepancy between this model and the actual behavior can be increased, since the real friction force exhibits a pronounced Stribeck effect at low speeds [11, 12]. Thus, extra attention should be paid to make more effective compensation for the nonlinear friction in order to enhance the control performance of multi-DOF hydraulic manipulator. Among the existing models, LuGre friction model [13] has been demonstrated to be effective in various actuation systems such as linear motors [14], PMSM servo systems [15] and hydraulic cylinders [16]. However, few studies can be found about applying LuGre model in hydraulic manipulators. Considering the complex dynamics of hydraulic manipulator itself, designing a model-based controller is still challenging.

In addition to control precision, energy efficiency is also important for hydraulic manipulators [4]. In most hydraulic manipulators, each hydraulic cylinder is controlled by a single proportional or servo valve. The hydraulic circuit is quite straightforward, and such four-way valve ensures the stability of the internal dynamics within the hydraulic system [10]. However, the inlet and outlets orifices of the actuator is coupled strongly by the mechanical linkage of the valve spool. This linkage restricts the control to a single control input for a given actuator, which makes it unfeasible for energy saving. In the field of electro-hydraulics, independent metering technique has been a solution for addressing energy efficiency concerns [17]. With in independent metering systems, each actuator is

controlled by two independent valves at least, which enables independent metering of the inlet and outlet orifices. This additional control input facilitates simultaneous energy savings through strategic control design. Although in many researches direct pump control becomes a good choice when energy saving is a major concern [18], the control performance of independent metering system can be much better since the actuator is still controlled by the high-response proportional or servo valves [19]. Implementing independent metering systems in hydraulic manipulators could offer both superior control performance and improved energy efficiency. However, the corresponding control flexibility should be handled properly by the controller [20].

To achieve high precise motion tracking performance while improve the energy efficiency, motion control of the hydraulic manipulator driven by an independent metering system is studied. The hydraulic circuit is designed based on the independent metering technique and the dynamics of the system is modelled. Then, the desired load force ensuring the tracking performance is synthesized based on the adaptive robust control theory [10], additionally considering nonlinear friction compensation. To address the flexibility of the independent metering configuration, a mode selection method is proposed to determine the control objective for each cylinder chamber. Motion and pressure controllers are then designed for both chambers. Finally, the control performance is evaluated theoretically and validated through comparative simulations and experiments.

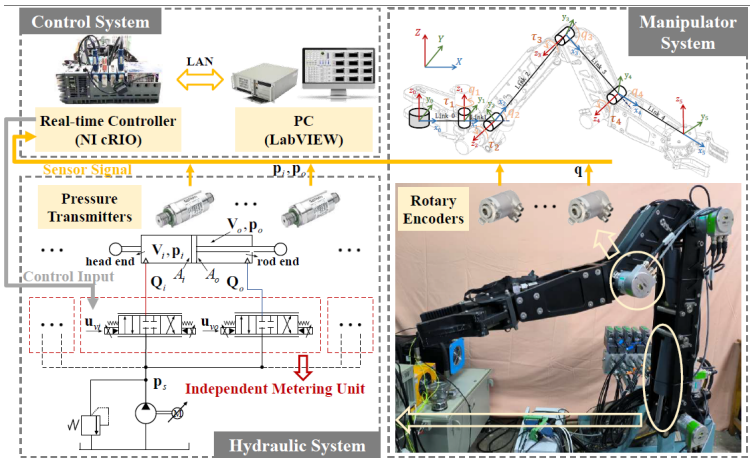

Figure 1: The common mechanism of multi-DOF hydraulic manipulator

2. HARDWARE CONFIGURATION AND PROBLEM FORMULATION

2.1. Hardware Configuration

A hydraulic manipulator with cylinders driving the joints is given in Fig. 1, illustrating the common mechanism of multi-DOF hydraulic manipulator. The corresponding coordinates are defined following the typical processes. Usually, each cylinder is controlled by a single four-way proportional or servo valve [4]. Instead, in this study, the independent metering technique is implemented in the hardware configuration. For example, for the n-th cylinder, two proportional four way valves, namely V_{in} and V_{on} are used coordinately to control the inlet and outlet flows, denoted as Q_{in} and Q_{on}, respectively. These two valves

collectively form an independent metering unit as shown in Fig. 1. It is important to mention that in independent metering systems, controlling the pump to match the flow required by the actuator is also crucial for energy savings. However, in this study, our primary focus will be on the control of independent metering valves.

2.2. Modeling of Hydraulic Manipulator

The model of the hydraulic manipulator is constructed as

$$\begin{aligned} &M(q)\ddot{q} + C(q,\dot{q})\dot{q} + G(q) = \tau + D_F \\ &\tau = J_h(q)F_L - T_f, F_L = A_i P_i - A_o P_o \end{aligned} \tag{1}$$

where $q \in \mathbb{R}^n$ is the joint angle. $M(q) \in \mathbb{R}^{n\times n}$, $C(q,\dot{q}) \in \mathbb{R}^{n\times n}$, and $G(q) \in \mathbb{R}^n$ denote the inertia matrix, the centripetal and Coriolis matrix, and the gravity terms, respectively. $D_F \in \mathbb{R}^n$ is the lumped modeling error including external disturbances and other hard-to-model terms, such as the non-uniform mass distribution across each link of the hydraulic manipulator. $J_h(q) \in \mathbb{R}^{n\times n}$ represents the nonsingular joint Jacobian matrix and $T_f \in \mathbb{R}^n$ means the friction torque. $F_L \in \mathbb{R}^n$ denotes the load force, with $A_i \in \mathbb{R}^{n\times n}$ and $A_o \in \mathbb{R}^{n\times n}$ being the head and rod-end ram areas of each cylinder. $P_i \in \mathbb{R}^n$ and $P_o \in \mathbb{R}^n$ represent the pressure of the two chambers, whose dynamics can be further expressed as

$$\begin{aligned} &V_i(x_L)\beta_{ei}^{-1}\dot{P}_i = -A_i\dot{x}_L + Q_i + D_{Qi} \\ &V_o(x_L)\beta_{eo}^{-1}\dot{P}_o = A_o\dot{x}_L - Q_o - D_{Qo} \end{aligned} \tag{2}$$

where $\dot{x}_L = J_h\dot{q}$, with x_L being the cylinder displacement. $\beta_{ei} \in \mathbb{R}$ and $\beta_{eo} \in \mathbb{R}$ denote the effective bulk modulus of the two chambers. $V_i(x_L) \in \mathbb{R}^{n\times n}$ and $V_o(x_L) \in \mathbb{R}^{n\times n}$ are the total compressible volumes of the head and rod end, respectively. $D_{Qi} \in \mathbb{R}^n$ and $D_{Qo} \in \mathbb{R}^n$ denote the lumped modeling errors, which include leakages in the hydraulic circuit and other minor nonlinear characteristics. Owing to the independent metering unit, Q_i and Q_o are two independent control inputs. In practice, Q_i and Q_o need to be reasonably distributed to obtain control signals for each valve core. Note that the dynamic response of the valve is much higher than other parts of the system, so only the static mapping of Q_i and Q_o to the valve control signal is considered. Therefore, this step will be omitted in the modeling process in this paper, and the general problem of controlling the motion of hydraulic manipulator with Q_i and Q_o will be studied.

The friction torque T_f is given by

$$T_f = Z\sigma_s + \dot{Z}\bar{\sigma}_m(\dot{q}) + \breve{\dot{q}}f_v, \dot{Z} = \dot{q} - \left|\dot{q}\right| g^{-1}(\dot{q})Z \tag{3}$$

where $Z \in \mathbb{R}^{n\times n}$ means the internal friction state and $\breve{\dot{q}} = diag(\dot{q})$. $\sigma_s \in \mathbb{R}^n$, $\bar{\sigma}_m(\dot{q}) = h_m(\dot{q})\sigma_m \in \mathbb{R}^n$, and $f_v \in \mathbb{R}^n$ are the stiffness, a velocity dependent damping coefficient, and the viscous friction coefficient, respectively. $g(\dot{q}) \in \mathbb{R}^{n\times n}$ is a positive diagonal matrix describing the Stribeck effect, in which

$$g_i(\dot{q}_i) = \alpha_{ci} + (\alpha_{si} - \alpha_{ci})e^{-(\dot{q}_i/\dot{q}_{si})^2} \tag{4}$$

with $\sigma_{si}\alpha_{si}$ and $\sigma_{si}\alpha_{ci}$ corresponding to the static friction and the Coulomb friction, respectively. $\dot{q}_{si}$ is the Stribeck velocity.

In addition, though the lumped modeling error $D_\bullet$ in (1) and (2) is unknown and time-varying, it can be split into the nominal value $D_{\bullet n}$ with slow variation and the bounded deviation value $\Delta D_\bullet$, i.e., $D_\bullet$ can be further denoted by

$$\begin{aligned} D_F &= D_{Fn} + \Delta D_F \\ D_{Qi} &= D_{Qin} + \Delta D_{Qi} \\ D_{Qo} &= D_{Qon} + \Delta D_{Qo} \end{aligned} \tag{5}$$

Property 1. The inertia matrix $M(q)$ is a positive definite symmetric matrix, and satisfies

$$\underline{\lambda}_M I_n \le M(q) \le \overline{\lambda}_M I_n \tag{6}$$

with $\underline{\lambda}_\bullet$ and $\overline{\lambda}_\bullet$ being the minimum and maximum eigenvalues of $\bullet$, respectively.

Property 1. The matrix $N(q,\dot{q}) = \dot{M}(q) - 2C(q,\dot{q})$ is skew-symmetric and

$$\dot{M}(q) = C(q,\dot{q}) + C^T(q,\dot{q}) \tag{7}$$

2.3. Dynamics parameterizing

For the convenience of subsequent controller derivation, the model in Section 2.1 can be parameterized as

$$\begin{aligned} M\ddot{q} + C\dot{q} &= J_h F_L - G - T_f(Z, \vartheta_{s1}) + \theta_4 + \Delta D_F \\ V_i(x_L)\theta_5 \dot{P}_i &= -A_i \dot{x}_L + Q_i + \theta_6 + \Delta D_{Qi} \\ V_o(x_L)\theta_7 \dot{P}_o &= A_o \dot{x}_L - Q_o - \theta_8 - \Delta D_{Qo} \end{aligned} \tag{8}$$

where $\vartheta_{s1} \triangleq [\theta_1^T, \theta_2^T, \theta_3^T, \theta_4^T]^T$, $\vartheta_{s2} \triangleq [\theta_5^T, \theta_6^T]^T$, and $\vartheta_{s3} \triangleq [\theta_7^T, \theta_8^T]^T$, in which θ_j means the parameter set of the j^{th} dynamics parameter at each joint, that is

$$\begin{aligned} \theta_j &= [\pi_1(j), \cdots, \pi_i(j), \cdots, \pi_n(j)]^T \\ \pi_i &= [\sigma_{si}, \sigma_{mi}, f_{vi}, D_{Fni}, , \beta_{ei}^{-1}, D_{Qini}, \beta_{eo}^{-1}, D_{Qoni}]^T \end{aligned} \tag{9}$$

with $\pi_i(j)$ being the j^{th} element of π_i. $T_f(\dot{q}, \vartheta_{s1}) = \phi_f^T \vartheta_{s1}$, and $\phi_f^T = \left[Z, \dot{Z}\, h_m, \breve{\dot{q}}, 0_{n\times 1} \right]$ is a linear regression matrix.

Assumption 1. The bounds of parametric uncertainties and uncertain nonlinearities are known, i.e.,

$$\vartheta_{si} \in \Omega_{\vartheta_{si}} \triangleq \{\vartheta_{si} : \vartheta_{si\min} \le \vartheta_{si} \le \vartheta_{si\max}\}$$
$$|\Delta D_F| \le \delta_F, |\Delta D_{Qi}| \le \delta_{Qi}, |\Delta D_{Qo}| \le \delta_{Qo} \tag{10}$$

where $\vartheta_{si\min}$, $\vartheta_{si\max}$, δ_F, δ_{Qi}, and δ_{Qo} are known scalars.

2.4. Control Objectives

Since independent metering technique is used for hydraulic manipulator, the controller should achieve high tracking performance while effectively managing the additional flexibility to enhance energy efficiency. The dual design objectives can be specifically described as:

1) High precision motion control: given a set of desired trajectories $q_d(t)$, the primary objective is to synthesize the valve spool voltage u_v, so that each joint angle $q(t)$ can track $q_d(t)$ as closely as possible, especially under low-speed conditions.

2) Low energy consumption: utilize the dual independent control valves for each actuator to maintain chamber pressures at low levels to conserve energy.

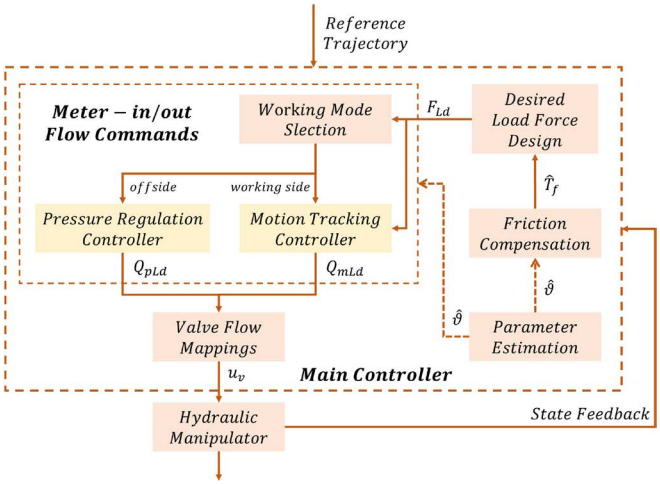

Figure 2: The overall control framework.

3. CONTROLLER DESIGN

In order to achieve the dual control objectives, the working mode selection is applied following the standard procedures proposed in [21]. In the selected working mode, the offside (to keep the chamber at a low pressure) and working side(motion tracking) independently control the pressure of the two chambers based on adaptive robust control theory [10]. The specific control framework is shown in Fig. 2.

The following notations are used throughout this paper: $\hat{\bullet}$ denotes the estimate of $\bullet$ and $\tilde{\bullet} = \hat{\bullet} - \bullet$ denotes the parameter estimation error.

3.1. Desired Load Force Design

This subsection aims to achieve motion tracking of the hydraulic manipulator and calculate the desired load force of the hydraulic cylinder F_{Ld} so that the angle tracking error $e_1 = q - q_d$ can be kept as small as possible.

Define a switching-function-like quantity

$$e_2 = \dot{e}_1 + K_1 e_1 = \dot{q} - \dot{q}_{eq}, \dot{q}_{eq} \triangleq \dot{q}_d - K_1 e_1 \tag{11}$$

with K_1 being a positive gain matrix. As long as the $e_2 \to 0$, the tracking error e_1 will be very small or converge to zero.

Differentiating (11) and noting (8), it has

$$\begin{aligned} M\dot{e}_2 + Ce_2 = J_h F_{Ld} + J_h e_3 - G - T_f(Z, \vartheta_{s1}) \\ +\theta_4 + \Delta D_F - (M\ddot{q}_{eq} + C\dot{q}_{eq}) \end{aligned} \tag{12}$$

with $e_3 = F_L - F_{Ld}$.

Considering that Z is unmeasurable, a dual observer based on mapping functions is designed as

$$\begin{aligned} \dot{\hat{z}}_1 &= \mathrm{Proj}_{\hat{z}_1}\left\{ x_2 - \frac{|x_2|}{g(x_2)}\hat{z}_1 - \gamma_1 e_2 \right\} \\ \dot{\hat{z}}_2 &= \mathrm{Proj}_{\hat{z}_2}\left\{ x_2 - \frac{|x_2|}{g(x_2)}\hat{z}_2 + \gamma_2 \frac{h(x_2)|x_2|}{g(x_2)} e_2 \right\} \end{aligned} \tag{13}$$

The virtual control force F_{Ld} can be designed as

$$\begin{aligned} F_{Ld} &= F_{Lda} + F_{Lds} \\ F_{Lda} &= F_{Lda1} + F_{Lda2},\ F_{Lds} = F_{Lds1} + F_{Ldas2} \\ F_{Lda1} &= J_h^{-1}\left(M\ddot{q}_{eq} + C\dot{q}_{eq} + G + \hat{T}_f(\hat{Z}, \hat{\vartheta}_{s1}) - \hat{\theta}_4 \right) \\ F_{Lds1} &= -J_h^{-1} K_{2s1} e_2, F_{Lds2} = -J_h^{-1} K_{2s2} e_2 \end{aligned} \tag{14}$$

in which K_{2s1} is a sufficiently large nonlinear gain matrix.

Consolidate the model compensation errors resulting from uncertain nonlinearities and physical parameter estimation discrepancies, and then separate them into a static component d_1 and a high-frequency component $d_1^*(t)$

$$d_1 + d_1^*(t) \triangleq \Delta D_F - \phi_F^T \tilde{\vartheta}_{s1} \tag{15}$$

Then, design fast dynamics compensation F_{Lda2} as

$$F_{Lda2} = -J_h^{-1}\hat{d}_1, \dot{\hat{d}}_1 = \mathrm{Proj}_{\hat{d}}(\gamma_F e_2) \tag{16}$$

in which γ_F is a positive constant matrix, and $\mathrm{Proj}_{\hat{d}}(\bullet)$ is a projection mapping.

K_{2s2} is a nonlinear robust feedback gain chosen large enough such that F_{Lds2} satisfies the following robust performance conditions:

$$
\begin{aligned}
&(i)\ \ e_2^T J_h F_{Lds2} \le 0 \\
&(ii)\ e_2^T (J_h F_{Lds2} - \tilde{d}_1 + \tilde{d}_1^* \\
&\qquad + \theta_1 \bar{Z}_1 - \theta_2 h_m \left|\dot{q}\right| g^{-1} \bar{Z}_2) \le \eta_1
\end{aligned} \tag{17}
$$

with $\eta_1 > 0$ being an arbitrarily small parameter.

Using (14) and (16), the resulting error dynamics of e_2 can be written as

$$
\begin{aligned}
M\dot{e}_2 + Ce_2 = &-K_{2s1}e_2 + \theta_1 \bar{Z}_1 - \theta_2 h_m \left|\dot{q}\right| g^{-1} \bar{Z}_2 \\
&+ J_h e_3 + \left(J_h F_{Lds2} - \tilde{d}_1 + \bar{d}_1^*\right)
\end{aligned} \tag{18}
$$

3.2. Pressure Regulation Controller

Hydraulic cylinders need to generate the desired load force mentioned above to achieve motion control goals, but the independent form of the load port allows for independent control of the pressure in both chambers, resulting in countless combinations of chamber pressures. According to the direction of the load force, when a forward load force is required, the pressure in the rod end chamber is controlled at a small value, while when a reverse load force is required, the pressure in the head chamber is controlled at a small value p_c, which can effectively achieve the goal of maintaining low pressure [21]. This subsection takes the rod end chamber as the offside as an example to design a pressure regulation controller. The pressure design for the head chamber follows the same procedure and is omitted here.

Define the tracking error of pressure as $e_{3p} = P_o - p_c$. The error dynamics would be the same as the pressure dynamics because p_c is constant

$$
\theta_7 \dot{e}_{3p} = V_o^{-1}\left(A_o \dot{x}_L - Q_o - \theta_8 - \Delta D_{Qo}\right) \tag{19}
$$

with Q_o being the control input, the proposed control law is given by

$$
\begin{aligned}
Q_{oLd} &= Q_{oLda} + Q_{oLds} \\
Q_{oLda} &= Q_{oLda1} + Q_{oLda2} \\
Q_{oLds} &= Q_{oLds1} + Q_{oLdas2} \\
Q_{oLda1} &= A_o \dot{x}_L - \hat{\theta}_8,\ \ Q_{oLda2} = V_o \hat{d}_p \\
Q_{oLds1} &= K_{os1} V_o e_{3p},\ \ Q_{oLds2} = K_{os2} V_o e_{3p}
\end{aligned} \tag{20}
$$

where Q_{oLda1} is the model compensation term and $\hat{d}_p$ is a fast dynamics compensation with $d_p + \bar{d}_p^*(t) \in V_o^{-1}\left(\tilde{\theta}_8 - \Delta D_{Qo}\right)$ and $\dot{\hat{d}}_p = \mathrm{Proj}_{\hat{d}}(\gamma_{Qo} e_{3p})$. $K_{os1} > 0$ and K_{os2} is a nonlinear feedback gain chosen to satisfy the following condition for performance robustness to model uncertainties:

$$
\begin{aligned}
&(i)\ \ -e_{3p}^T V_o^{-1} Q_{oLds2} \le 0 \\
&(ii)\ e_{3p}^T \left(-V_o^{-1} Q_{oLds2} - \tilde{d}_p + \bar{d}_p^*\right) \le \eta_p
\end{aligned} \tag{21}
$$

with $\eta_p > 0$ being an arbitrarily small parameter.

Substituting control law (20) into (19), the error dynamics can be written as

$$\theta_7 \dot{e}_{3p} = -K_{os1} e_{3p} + \left(\bar{d}_p^* - \tilde{d}_p - V_o^{-1} Q_{oLds2} \right) \tag{22}$$

3.3. Motion Tracking Controller

The pressure regulation controller has already calculated the control flow Q_{oLd}. Furthermore, it is necessary to calculate the control flow rate based on the desired load force to achieve accurate motion tracking in the closed-loop system.

The error between the real load force and the desired load force is $e_{3m} = F_L - F_{Ld}$, whose derivative is

$$\begin{aligned} \theta_5 \dot{e}_{3m} &= \theta_5 \dot{F}_L - \theta_5 \dot{F}_{Ld} \\ &= -(V_i^{-1} A_i^2 + V_o^{-1} A_o^2) \dot{x}_L + V_i^{-1} A_i Q_i + V_o^{-1} A_o Q_o \\ &\quad + V_i^{-1} A_i \theta_6 + V_o^{-1} A_o \theta_8 + A_i \Delta D_{Qi} - A_o \Delta D_{Qo} - \dot{F}_{Ld} \end{aligned} \tag{23}$$

where $\dot{F}_{Ld}$ can be further expressed as the incalculable part $\dot{F}_{Ldi}$ and calculable part $\dot{F}_{Ldc}$.

Similar to Q_{oLd}, Q_{iLd} in (23) can be generated as

$$\begin{aligned} &Q_{iLd} = Q_{iLda} + Q_{iLds} \\ &Q_{iLda} = Q_{iLda1} + Q_{iLda2} \\ &Q_{iLds} = Q_{iLds1} + Q_{iLdas2} \\ &Q_{iLda1} = V_i A_i^{-1} [(V_i^{-1} A_i^2 + V_o^{-1} A_o^2) \dot{x}_{\mathrm{L}} - V_o^{-1} A_o Q_o \\ &-V_i^{-1} A_i \hat{\theta}_6 - V_o^{-1} A_o \hat{\theta}_8 + \dot{F}_{\mathrm{Ldc}} + \mathrm{Y}_{Qm}] \\ &Q_{iLda2} = -V_i A_i^{-1} \hat{d}_m \\ &Q_{iLds1} = -k_{\mathrm{is1}} V_i A_i^{-1} e_{3m},\ Q_{iLds2} = -k_{\mathrm{is2}} V_i A_i^{-1} e_{3m} \end{aligned} \tag{24}$$

with k_{is1} being a gain matrix and $\mathrm{Y}_{Qm} = -\omega_1 \omega_2^{-1} J_h e_2$. $\hat{d}_m$ is a fast dynamics compensation with $\dot{\hat{d}}_m = \mathrm{Proj}_{\hat{d}}(\gamma_{Qi} e_{3m})$. k_{is2} is a nonlinear robust feedback gain chosen large enough such that Q_{Lds2} satisfies the following robust performance conditions:

$$\begin{aligned} &(i)\ \ e_{3m}^T Q_{iLds2} \le 0 \\ &(ii)\ e_{3m}^T \left(V_o^{-1} A_o Q_{iLds2} - \tilde{d}_2 + \bar{d}_2^* \right) \le \eta_m \end{aligned} \tag{25}$$

with $\eta_m > 0$ being an arbitrarily small parameter.

Substituting control law (24) into (23), the error dynamics can be written as

$$\dot{e}_{3m} = -k_{\mathrm{is1}} z_3 + \left(V_o^{-1} A_o Q_{Lds2} - \tilde{d}_2 + \bar{d}_2^* \right) + \mathrm{Y}_{Qm} \tag{26}$$

3.4. Parameter Estimation

The parameter estimation law is given as

$$\dot{\hat{\vartheta}}_{si} = \mathrm{sat}_{\hat{\vartheta}}(\mathrm{Proj}_{\hat{\vartheta}}(\Gamma_i \tau_i)) \tag{27}$$

The projection function $\mathrm{Proj}_{\hat{\vartheta}}(\bullet)$ is defined as

$$\mathrm{Proj}_{\hat{\vartheta}}(\bullet)=\begin{cases}\bullet, & \hat{\vartheta}\in\Omega_{\vartheta}\ \text{or}\ n_{\hat{\vartheta}}^{T}\bullet\le 0\\ \left(I-\Gamma\dfrac{n_{\hat{\vartheta}}n_{\hat{\vartheta}}^{T}}{n_{\hat{\vartheta}}^{T}\Gamma n_{\hat{\vartheta}}}\right)\bullet, & \hat{\vartheta}\in\partial\Omega_{\vartheta}\ \text{and}\ n_{\hat{\vartheta}}^{T}\bullet\ge 0\end{cases} \tag{28}$$

where Ω_{ϑ}, $\partial\Omega_{\vartheta}$, and $n_{\hat{\vartheta}}$ are the interior and the boundary of Ω_{ϑ} and the outward unit normal vector at $\hat{\vartheta}\in\partial\Omega_{\vartheta}$.

Define regressors as

$$\begin{aligned}\phi_1^T &= \left[-Z_d, -\dot{Z}_d\ h_m, -\dot{q}, I_{n\times 1}\right]\\ \phi_2^T &= [-\dot{P}_i, V_i^{-1}]^T\\ \phi_3^T &= [-\dot{P}_o, -V_o^{-1}]^T\\ u_1 &= J_h F_L - M\ddot{q} - C\dot{q} - G\\ u_2 &= V_i^{-1}(-A_i\dot{x}_L + Q_i)\\ u_3 &= V_o^{-1}(A_o\dot{x}_L - Q_o)\end{aligned} \tag{29}$$

A stable filter $H_f(s)$ with a relative degree no less than one is used to handle the sensor noise. Noting (29) we can get

$$u_{if} = -\phi_{if}^T\vartheta_{is} \tag{30}$$

Define the prediction out and prediction error as

$$\begin{aligned}\hat{u}_{if} &= \phi_{if}^T\hat{\vartheta}_{is}\\ \dot{\varsigma}_i &= \hat{u}_{if} - u_{if} = \phi_{if}^T\tilde{\vartheta}_{is}\end{aligned} \tag{31}$$

$\Gamma_i(t)$ is updated by

$$\dot{\Gamma}_i=\begin{cases}\alpha\Gamma_i-\Gamma_i\phi_{if}\phi_{if}^T\Gamma_i, & \text{if } \lambda_{\max}(\Gamma_i(t))\le\rho_M\\ 0, & \text{else}\end{cases} \tag{32}$$

in which ρ_M is the upper bound of $\Gamma_i(t)$, α is the forgetting factor, and $\nu\ge 0$. The adaptation function $\tau_i=\phi_{if}\dot{\varsigma}_i$.

Theorem 1. All signals in the system controller are bounded. Furthermore, the positive-definite function V_s defined by

$$V_s=\frac{1}{2}e_1^Tw_1K_1^2e_1+\frac{1}{2}e_2^Tw_1Me_2+\frac{1}{2}e_{3m}^T\theta_5e_{3m}+\frac{1}{2}e_{3p}^Tw_2\theta_7e_{3p} \tag{33}$$

is bounded above by

$$V_s(t)\le\exp(-\lambda_s t)V_s(0)+\frac{\eta_s}{\lambda_s}\left[1-\exp\left(-\lambda_s t\right)\right] \tag{34}$$

with $\lambda_s=\min\left\{\underline{\lambda}_{K_1}, 2\underline{\lambda}_{K_{2s1}}/\overline{\lambda}_M, 2\underline{\lambda}_{K_{is1}}/\theta_{5max}, 2\underline{\lambda}_{K_{os1}}/\theta_{7max}\right\}$ and $\eta_s=w_1\eta_1+w_2\eta_m+\eta_p$. In addition, if there is only parameter uncertainties in the system after a finite time, the

closed-loop system can achieve asymptotic tracking performance, i.e., the tracking errors $e_1 \to 0 \quad \text{as} \, t \to \infty$.

4. SIMULATIONS AND EXPERIMENTS

To verify the feasibility and effectiveness of the proposed control strategy, both simulations and experiments were conducted. The simulations were designed to evaluate the controller performance under controlled and reproducible conditions, while the experiments further validated its applicability in real hardware environments.

4.1. Simulations

In the simulation, the multi-DOF coupling effect, sensor measurement noise, and the dynamic process of the valve simulated by a second-order system are all considered, to make it more practical. The noises of the angle encoder is set as $1\times10^{-4} rad$, which is consistent with reality.

Two controllers were compared to highlight the advantages of the proposed method as follows:.

C1: the proposed controller with the LuGre model compensation, enabling better handling of nonlinear friction, particularly at low velocities. The control law can be represented by (14), (20), (24).

C2: the proposed controller with the Coulomb and viscous friction model, which is widely used [22]. The only difference from C1 is that the friction compensation term is composed of $\hat{T}_f = S_a(\dot{q})\hat{\theta}_3 + \dot{q}\,\hat{\theta}_4$.

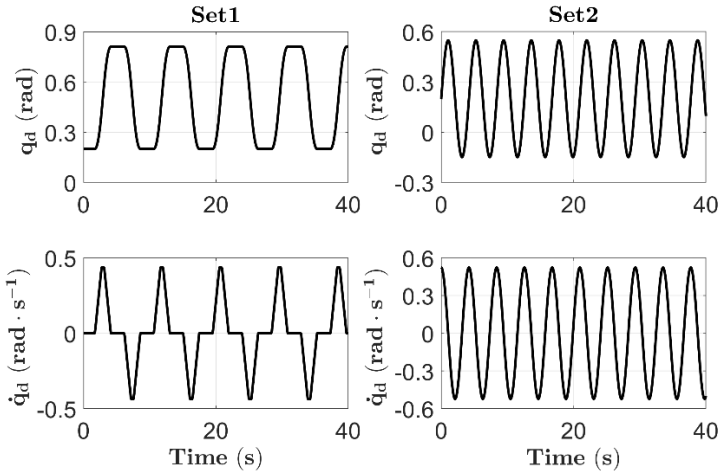

Figure 3: The reference trajectories.

Two sets of experiments, as show in Fig.3, were set up as follows:

Set1: Slow point-to-point(P2P) tracking experiment. The desired trajectory was from 0.2rad to 0.81rad, with the maximum angular velocity 0.43rad/s, which includes various motion states such as starting, accelerating, constant speed, and decelerating.

Set2: Slow SINE curve tracking experiment. The desired trajectory was set as $q_d(t) = 20\sin(1.5t)\,\text{rad}$.

In the simulation, all joints are controlled by the proposed method to track the reference trajectory simultaneously. For clarity, the analysis here focuses solely on the swing joint. To rigorously evaluate the tracking accuracy, quantitative metrics including the maximum tracking error e_{max} and the Integral of Time-weighted Absolute Error (ITAE) were introduced. The ITAE index is particularly significant as it penalizes long-duration errors, thereby reflecting the steady-state accuracy and convergence speed.

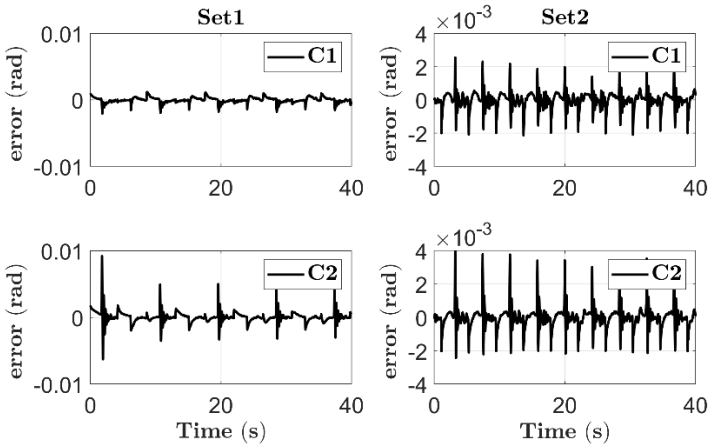

Figure 4: The tracking errors of C1 and C2.

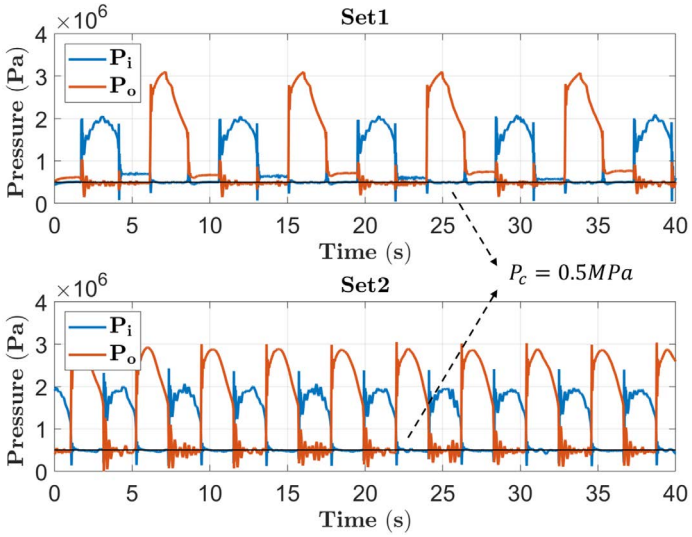

Figure 5: The pressure regulation results of C1.

The experiment results are shown in Fig. 4, and Table 1 is a summary of the comparison results. In the Point-to-Point motion (Set1), which involves frequent acceleration and deceleration phases, the proposed adaptive robust controller (C1) demonstrated remarkable performance. Specifically, C1 reduced the maximum tracking error e_{max} by 77.73% (from 0.0092 rad to 0.0020 rad) compared to the traditional controller (C2). This substantial reduction indicates that the proposed LuGre model-based friction compensation effectively

suppresses the error spikes caused by the Stribeck effect during zero-speed crossings. Furthermore, the ITAE index was reduced by 27.44%, confirming improved global tracking capability. Similarly, in the continuous Sine wave tracking (Set2), C1 consistently outperformed C2, achieving a 41.94% reduction in peak error and a 13.87% reduction in ITAE. These quantitative improvements validate that the proposed strategy not only handles nonlinear friction more effectively but also achieves higher precision across different motion trajectories. In addition, the pressure regulation results of C1 are show in Fig. 5, where the pressures of both chambers are regulated at a low level, which means the energy efficiency can be further improved by the independent metering technique.

Table 1: Quantitative comparison of tracking performance metrics.

Motion Set	Metric	C1	C2	Improvement
Set 1 (P2P)	e_{max} (rad)	0.0020	0.0092	77.73%
	ITAE ($rad \cdot s$)	0.2313	0.3188	27.44%
Set 2 (Sine)	e_{max} (rad)	0.0025	0.0044	41.94%
	ITAE ($rad \cdot s$)	0.2537	0.2946	13.87%

4.2. Experiments

The experimental validation was conducted on a customized 4-DOF hydraulic manipulator test rig (as shown in Fig. 1). The system is powered by a variable displacement pump station with a supply pressure of 10 MPa. The joint angles are measured by high-resolution rotary encoders, and the cylinder pressures are monitored by pressure sensors installed at both chambers to provide feedback for the pressure regulation loop. Real-time control algorithms are implemented on a NI cRIO system with the control frequency being 300 Hz. Compared with the simulation, additional real-world effects such as valve hysteresis, signal noise, and load fluctuations were present. The experimental results, as shown in Fig. 6, confirm that the proposed method effectively improves trajectory tracking accuracy, validating its potential for practical implementation in hydraulic manipulators.

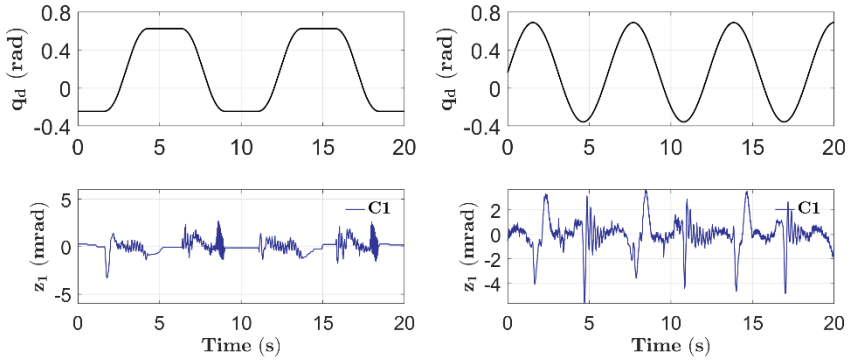

Figure 6: The experiment results of C1.

5. CONCLUSION

This paper presented a motion control strategy for a multi-DOF hydraulic manipulator driven by an independent metering system. An adaptive robust controller with LuGre

friction compensation was developed to handle system nonlinearities and uncertainties while improving energy efficiency. Both simulation and experimental results verified that the proposed method achieves high tracking accuracy and maintains low chamber pressures, demonstrating its potential for efficient and precise hydraulic manipulation.

6. REFERENCES

[1] Lee, M., Choi, H., Kim, C., Moon, J., Kim, D., and Lee, D., "Precision motion control of robotized industrial hydraulic excavators via data-driven model inversion," Proc. in IEEE Robotics and Automation Letters, vol. 7, no. 2, pp. 1912–1919, 2022.

[2] Zhou, S., Shen, C., Xia, Y., Chen, Z., and Zhu, S., "Adaptive robust control design for underwater multi-DOF hydraulic manipulator," Proc. in Ocean Engineering, vol. 248, p. 110822, 2022.

[3] Sivcev, S., Coleman, J., Omerdic, E., Dooly, G., and Toal, D., "Underwater manipulators: A review," Proc. in Ocean Engineering, vol. 163, pp. 431–450, 2018.

[4] Mattila, J., Koivumäki, J., Caldwell, D. G., and Semini, C., "A survey on control of hydraulic robotic manipulators with projection to future trends," Proc. in IEEE/ASME Transactions on Mechatronics, vol. 22, no. 2, pp. 669–680, 2017.

[5] Zhang, J., Zhang, F., Cheng, M., Ding, R., Xu, B., and Zong, H., "Parameter identification of hydraulic manipulators considering physical feasibility and control stability," Proc. in IEEE Transactions on Industrial Electronics, vol. 71, no. 1, pp. 718–728, 2024.

[6] Mohanty, A., and Yao, B., "Integrated direct/indirect adaptive robust control of hydraulic manipulators with valve deadband," Proc. in IEEE/ASME Transactions on Mechatronics, vol. 16, no. 4, pp. 707–715, 2010.

[7] Deng, W., Zhou, H., Zhou, J., and Yao, J., "Neural network-based adaptive asymptotic prescribed performance tracking control of hydraulic manipulators," Proc. in IEEE Transactions on Systems, Man, and Cybernetics: Systems, vol. 53, no. 1, pp. 285–295, 2022.

[8] Liang, X., Yao, Z., Deng, W., and Yao, J., "Adaptive control of n-link hydraulic manipulators with gravity and friction identification," Proc. in Nonlinear Dynamics, vol. 111, no. 20, pp. 19093–19109, 2023.

[9] Feng, H., Qiao, W., Yin, C., Yu, H., and Cao, D., "Identification and compensation of non-linear friction for an electro-hydraulic system," Proc. in Mechanism and Machine Theory, vol. 141, pp. 1–13, 2019.

[10] Yao, B., Bu, F., Reedy, J., and Chiu, G. T. C., "Adaptive robust motion control of single-rod hydraulic actuators: Theory and experiments," Proc. in IEEE/ASME Transactions on Mechatronics, vol. 5, no. 1, pp. 79–91, Mar. 2000.

[11] Pan, Q., Li, Y., and Huang, M., "Control-oriented friction modeling of hydraulic actuators based on hysteretic nonlinearity of lubricant film," Proc. in Mechatronics, vol. 53, pp. 72–84, 2018.

[12] Helian, B., Chen, Z., Yao, B., Lyu, L., and Li, C., "Accurate motion control of a direct-drive hydraulic system with an adaptive nonlinear pump flow compensation," Proc. in IEEE/ASME Transactions on Mechatronics, vol. 26, no. 5, pp. 2593–2603, 2020.

[13] Chen, P., Liu, X., and Yan, Q., "Adaptive friction compensation for a class of mechanical systems based on LuGre model," Proc. in International Journal of Robust and Nonlinear Control, vol. 32, no. 7, pp. 4510–4534, 2022.
[14] Lu, L., Yao, B., Wang, Q., and Chen, Z., "Adaptive robust control of linear motors with dynamic friction compensation using modified LuGre model," Proc. in Automatica, vol. 45, no. 12, pp. 2890–2896, 2009.
[15] Zhang, W., Li, M., Gao, Y., and Chen, Y., "Periodic adaptive learning control of PMSM servo system with LuGre model-based friction compensation," Proc. in Mechanism and Machine Theory, vol. 167, p. 104561, 2022.
[16] Dai, K., Zhu, Z., Shen, G., Tang, Y., Li, X., Wang, W., and Wang, Q., "Adaptive force tracking control of electrohydraulic systems with low load using the modified LuGre friction model," Proc. in Control Engineering Practice, vol. 125, p. 105213, 2022.
[17] Abuowda, K., Okhotnikov, I., Noroozi, S., Godfrey, P., and Dupac, M., "A review of electrohydraulic independent metering technology," Proc. in ISA Transactions, vol. 98, pp. 364–381, 2020.
[18] Chen, Z., Helian, B., Zhou, Y., and Geimer, M., "An integrated trajectory planning and motion control strategy of a variable rotational speed pump-controlled electro-hydraulic actuator," Proc. in IEEE/ASME Transactions on Mechatronics, vol. 28, no. 1, pp. 588–597, 2022.
[19] Lyu, L., Chen, Z., and Yao, B., "Advanced valves and pump coordinated hydraulic control design to simultaneously achieve high accuracy and high efficiency," Proc. in IEEE Transactions on Control Systems Technology, vol. 29, no. 1, pp. 236–248, 2020.
[20] Lyu, L., Chen, Z., and Yao, B., "Energy saving motion control of independent metering valves and pump combined hydraulic system," Proc. in IEEE/ASME Transactions on Mechatronics, vol. 24, no. 5, pp. 1909–1920, 2019.
[21] Liu, S., and Yao, B., "Coordinate control of energy saving programmable valves," Proc. in IEEE Transactions on Control Systems Technology, vol. 16, no. 1, pp. 34–45, 2008.
[22] Guo, Q., Wang, Q., and Liu, Y., "Antiwindup control of an electrohydraulic system with load disturbance and modeling uncertainty," Proc. in IEEE Transactions on Industrial Informatics, vol. 14, no. 7, pp. 3097–3108, 2018.

Biographies

Yangxiu Xia received the B.Eng. degree in ocean engineering and technology from Zhejiang University, Hangzhou, China, in 2022. He is currently working toward the Ph.D. degree in ocean technology and engineering with the Ocean College, Zhejiang University, Zhoushan, China.

Litong Lyu received the B.Eng. and Ph.D. degrees in mechatronics engineering from Zhejiang University, Hangzhou, China, in 2015 and 2020, respectively.

Since 2020, he has been with the School of Mechanical Engineering, Shijiazhuang Tiedao University, Hebei, China, where he is currently an Associate Professor.

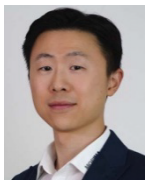

Bobo Helian received the B.Eng. degree in mechanical engineering from Yanshan University, Qinhuangdao, China, in 2015, and the Ph.D. degree in mechatronic engineering from Zhejiang University, Hangzhou, China, in 2021. Since 2021, he has been a Postdoctoral Researcher with the Institute of Mobile Machines, Karlsruhe Institute of Technology (KIT), Karlsruhe, Germany. His research interests include advanced controls of electro-hydraulic systems (e.g., motion control, machine learning, trajectory planning, constrained control, nonlinear adaptive robust control, energy-saving control, and independent metering control).

Zheng Chen received the B.Eng. and Ph.D. degrees in mechatronic control engineering from Zhejiang University, Hangzhou, China, in 2007 and 2012, respectively.

From 2013 to 2015, he was a Postdoctoral Researcher with the Department of Mechanical Engineering, Dalhousie University, Halifax, NS, Canada. Since 2015, he has been an Associated Professor with the Ocean College, Zhejiang University, Hangzhou. His research interests mainly focus on advanced control of robotic and mechatronic systems (e.g., nonlinear adaptive robust control, motion control, trajectory planning, telerobotics, exoskeleton, mobile manipulator, precision mechatronic systems, and underwater robots).